Batteries & Supercaps

Research Article
doi.org/10.1002/batt.202300516

Chemistry Europe
European Chemical Societies Publishing

www.batteries-supercaps.org

Cobalt/MXene-derived TiO_2 Heterostructure as a Functional Separator Coating to Trap Polysulfide and Accelerate Redox Kinetics for Reliable Lithium-sulfur Battery

Zhihua Chang[+],[a] Wendong Liu[+],[a] Junan Feng,[a] Zenghui Lin,[a] Chuan Shi,[a] Tianyi Wang,[c] Yaojie Lei,[d] Xiaoxian Zhao,*[b] Jianjun Song,*[a] and Guoxiu Wang*[d]

Lithium-sulfur (Li–S) batteries are one of the most potential new energy storage systems due to their high theoretical capacity (1675 mAh g^{-1}) and high energy density (2600 Wh kg^{-1}). However, the application of Li–S batteries is currently restricted due to the dissolution of polysulfides in the electrolyte, which leads to the shuttle effect of lithium polysulfides (LiPSs). Here, we present a Co@MXene-derived TiO_2 heterostructure decorated on carbon sheets derived from folic acid (Co@M-TiO_2/C) as a functional separator coating to trap polysulfide and accelerate redox kinetics in Li–S batteries. The interconnected porous structure with good electrical conductivity of the heterostructure boasts rapid ion diffusion and efficient electron transfer within the battery. By attaching Co and MXene-derived dual-phased TiO_2 to two-dimensional carbon sheets, heterostructures are formed, ensuring complete exposure of the active sites. These heterostructures exhibit catalytic effects on LiPSs and excellent adsorption capabilities, effectively inhibiting the shuttle effect and accelerating the redox kinetics. Considering these advantages, the Li–S battery with the optimized Co@M-TiO_2/C modified separator demonstrates a high specific capacity of 1481.7 mAh g^{-1} at 0.2 C, superior rate performance of 855.5 mAh g^{-1} at 2 C, and excellent cycling performance under a high sulfur load of 4.4 mg cm^{-2}.

Introduction

Among the different emerging energy storage systems that surpass the current lithium-ion batteries (LIBs),[1,2] lithium-sulfur (Li–S) battery is considered one of the most promising options for commercial use due to the high theoretical capacity of S (1675 mAh g^{-1}) and high energy density (2600 Wh kg^{-1}).[3,4] In addition, S is extremely abundant, non-toxic, and extremely friendly to the environment.[5] Even so, the practical application of Li–S batteries has faced various challenges.[6–8] These obstacles include the low electrical conductivity of S, the discharge product Li_2S,[9–11] and notable changes in volume during charging and discharging.[12,13] The growth of lithium dendrites is likely to lead to internal short circuits or even thermal runaway failure of the battery.[14] The shuttle effect is the most crucial challenge in Li–S batteries, as it entails the movement of polysulfide intermediates (Li_2S_n, where $4 \leq n \leq 8$) (LiPSs) that are dissolved in the electrolyte, which leads to the rapid capacity degradation and low Coulombic efficiency.[15–17] To address those challenges, researchers have carried out tremendous work to improve the conductivity of the entire electrode by designing carbon-based S cathode. Advanced S host materials have been designed to prevent the movement of LiPSs, which can employ as physical barriers or suppress LiPSs shuttle through physical or chemical adsorption.

In addition, to design an advanced modified separator can enhance the performance of Li–S batteries.[18–20] Such modified separators are easy to prepare and can serve as a barrier to inhibit the LiPSs shuttle effect, as well as a storage unit for various sulfides. Several materials have been developed to hinder the movement of LiPSs intermediates toward the cathode, including various carbon materials superconductive carbon black, acetylene black,[21] graphene,[22] and multi-walled carbon nanotubes,[23] which are for the large specific surface area, and excellent conductivity. Moreover, polar materials, such as metal oxides,[24,25] metal sulfides,[26,27] metal nitrides,[28] metal phosphides,[29,30] metal selenides,[31] and metal simple substances,[32] can provide strong chemical adsorption to LiPSs

[a] Z. Chang,[+] W. Liu,[+] J. Feng, Z. Lin, Prof. C. Shi, Prof. J. Song
College of Physics
Qingdao University
Qingdao 266071, P. R. China
E-mail: jianjun.song@qdu.edu.cn

[b] Prof. X. Zhao
Department of Chemistry, College of Science
Hebei Agricultural University
Baoding 071001, P. R. China
E-mail: lxzhxx@hebau.edu.cn

[c] Prof. T. Wang
School of Chemistry and Chemical Engineering
Yangzhou University
Yangzhou 225002, P. R. China

[d] Y. Lei, Prof. G. Wang
Centre for Clean Energy Technology
University of Technology Sydney
Broadway, Sydney, NSW 2007, Australia
E-mail: Guoxiu.Wang@uts.edu.au

[+] These authors contributed equally to this work.

Supporting information for this article is available on the WWW under https://doi.org/10.1002/batt.202300516

Research Article
doi.org/10.1002/batt.202300516
Chemistry Europe
European Chemical Societies Publishing

and catalyze their transformation.[33] Among them, cobalt is considered to have favorable adsorption of LiPSs and brilliant catalytic LiPSs conversion ability and has excellent electrical conductivity, which is widely used in the modification of Li–S batteries.[34]

MXenes, as a novel 2D layered material, have been widely studied in Li–S batteries owing to their excellent electronic conductivity, hydrophilicity, 2D polar surfaces, and catalytic conversion capabilities.[35,36] $Ti_3C_2T_x$ can be easily converted to TiO_2 and C after simple heat treatment, which exhibits admirable adsorption and catalytic capabilities to LiPSs, suppressing shuttle effects, and improving reaction kinetics.[37] Therefore, it will be highly potential to explore the incorporation of MXene-derived TiO_2 and Co to overcome the shortcomings of Li–S batteries.

In this work, we prepared a novel Co and MXene-derived TiO_2 heterostructure decorated on folic acid-derived carbon sheet (Co@M-TiO_2/C) by a facile hydrothermal method and calcination as a functional separator coating to trap polysulfide and accelerate redox kinetics for Li–S batteries. (Figure 1). The interconnected porous carbon sheet structure with good electrical conductivity and high specific surface area endows the batteries with rapid ion diffusion and fast electron transfer. Co is attached to the two-dimensional carbon sheets together with MXene-derived TiO_2 to form a heterostructure to ensure the full exposure of active sites, and the unique point-to-interfaces mode enables strong chemical interaction and catalytic property to LiPSs, thus effectively constraining the shuttle effect and accelerating the redox kinetics. Thus, the Li–S battery with optimum Co@M-TiO_2/C modified separator shows a high specific capacity, excellent cycling performance under high load, and ascendant rate performance.

Results and Discussion

The microstructure of Co@M-TiO_2/C samples is observed by scanning electron microscope (SEM). The SEM images (Figure 2a–f) display that all the Co@M-TiO_2/C samples possess a unique interconnected porous structure composed of crinkled and thin sheets, which provides more exposed active sites and a larger LiPSs contact area. Co/C also shows a similar porous structure (Figure S1a–d), indicating that the introduction of MXene does not cause obvious morphological changes due to its ultra-thin two-dimensional structure. The transmission electron microscope (TEM) images (Figure 2g) confirm the ultrathin

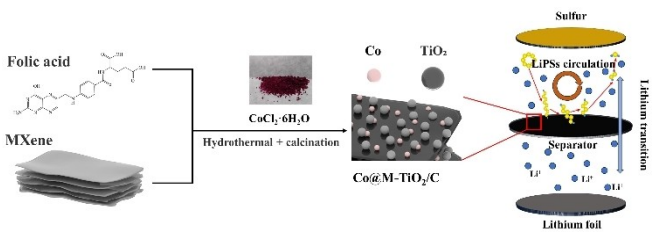

Figure 1. Schematic of the preparation process of Co@M-TiO_2/C and the transformation process of LiPSs on Co@M-TiO_2/C surface.

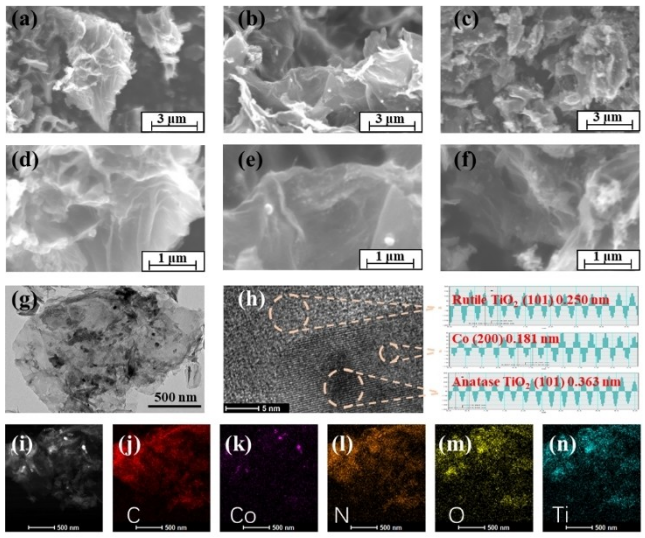

Figure 2. Different resolutions of SEM images of Co@M-TiO_2/C-1 (a, d), Co@M-TiO_2/C-2 (b, e), Co@M-TiO_2/C-3 (c, f). TEM images of Co@M-TiO_2/C-2 (g). HR-TEM image of Co@M-TiO_2/C-2 (h). HADDF-STEM of Co@M-TiO_2/C-2 (i). Elemental mapping image of C, Co, N, O, and Ti in a selected area of Co@M-TiO_2/C-2 (j-n).

structure of Co@M-TiO_2/C-2 and many active nanoparticles are attached to its surface. Through high-resolution TEM (HRTEM) images of the particles (Figure 2h, S2), the lattice spacing of 0.181 nm corresponds to the (200) crystal plane of Co, the lattice spacing of 0.250 nm corresponds to the (101) crystal plane of Rutile TiO_2, and the lattice spacing of 0.363 nm corresponds to the (101) crystal plane of Anatase TiO_2, demonstrating the formation of the Co@M-TiO_2 heterostructure, which facilitates the fast conversion of LiPSs and promotes the electron transfer. The high-angle annular dark field SEM (HAADF-STEM) image (Figure 2i) and the EDS map of Co@M-TiO_2/C-2 (Figure 2j-n) show the characteristic elements (C, Co, N, O, Ti) are uniformly distributed in Co@M-TiO_2/C-2. In the cross-sectional SEM image (Figure S3), the thickness of the Co@M-TiO_2/C-2 and Co/C functional layer on the separator is 4.411 μm and 5.767 μm, respectively.

X-ray diffraction (XRD) patterns reveal the material composition of Co@M-TiO_2/C and Co/C (Figure 3a). For Co/C sample, only characteristic peaks of Co were detected. In the XRD patterns of Co@M-TiO_2/C composites, several main characteristic peaks in agreement with MXene-derived dual-phased TiO_2 (Antase: PDF#21-1272, Rutile: PDF#21-1276) and Co (PDF#15-0806) are detected, demonstrating the successful co-existence of Co and M-TiO_2. The chemical state and composition of the samples are measured by X-ray photoelectron spectroscopy (XPS). In the High-resolution XPS (HRXPS) spectrum of Co 2p (Figure 3b), two peaks distinguished at 781.33 eV and 798.61 eV can be attributed to the Co in Co@M-TiO_2/C. The HRXPS spectrum of N 1s can be fitted to pyrrole nitrogen (399.19 eV), pyridine nitrogen (398.25 eV), and graphite nitrogen (401.02 eV) (Figure 3c). In the HRXPS spectrum of Ti 2p (Figure 3d), two peaks can be distinguished at 458.52 eV and 464.28 eV which belong to M-TiO_2. The HRXPS spectrum of Co/C (Figure **S**4)

Research Article
doi.org/10.1002/batt.202300516

Chemistry Europe
European Chemical Societies Publishing

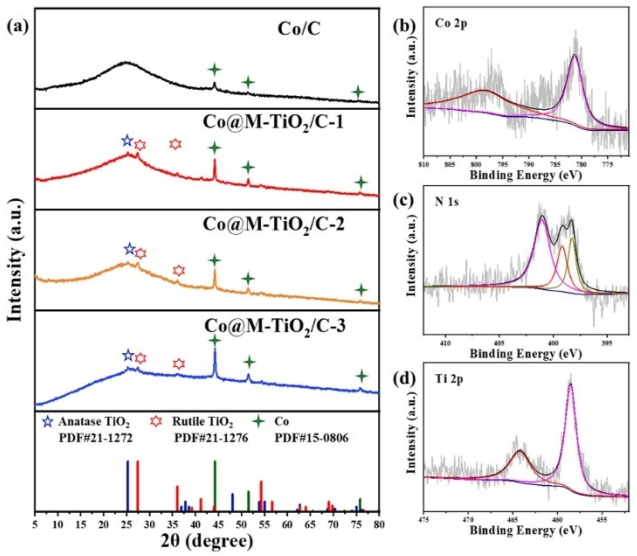

Figure 3. The XRD patterns of Co/C and Co@M-TiO_2/C samples (a). The XPS spectra of Co@M-TiO_2/C-2 of Co 2p (b), N 1s (c), Ti 2p (d).

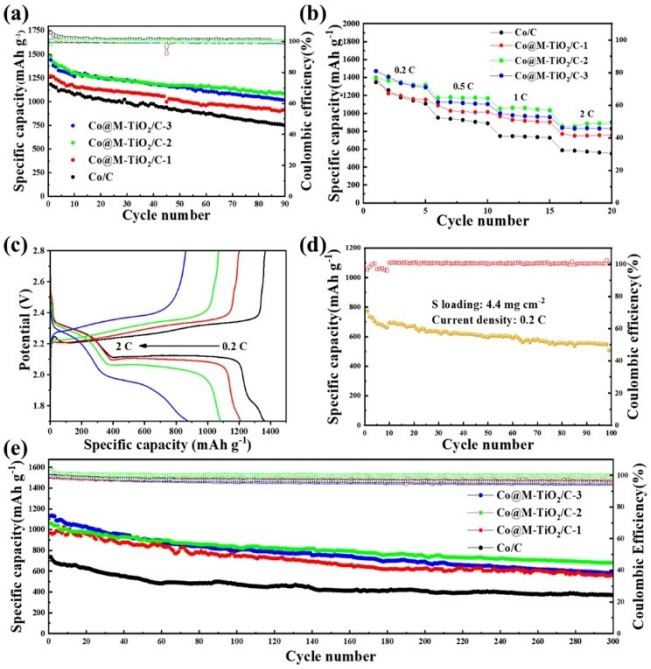

Figure 4. (a) Cycling performance at 0.2 C. (b) Rate performance. (c) Discharge/charge profiles of the cell with Co@M-TiO_2/C-2 modified separator at different rates (0.2 C, 0.5 C, 1 C, and 2 C). (d) High-loading cycling performance of the batteries with Co@M-TiO_2/C-2 separator. (e) Long-term cycling performance at 1 C.

shows two characteristic peaks of 780.89 eV and 796.79 eV in the Co 2p image, which are mutually confirmed with the crystal phase of the Co simple substance in XRD. There are three characteristic peaks corresponding to pyridine nitrogen (398.13 eV), pyrrole nitrogen (398.85 eV), and graphite nitrogen (400.95 eV) in the N 1s spectrum. The results of XRD and XPS confirmed the successful preparation of the Co@M-TiO_2/C composites.

The CR2032 cells with Co@M-TiO_2/C and Co/C modified separators were assembled to test the influence of Co@M-TiO_2/C on the performance of Li–S batteries. The Ketjen black/sulfur (KB/S) composites were used as cathode materials and the S content is calculated to be 73.81 % according to the thermogravimetric test (Figure **S**5). Figure 4a displays the cycling stability of the cells with Co@M-TiO_2/C and Co/C separators. The Co@M-TiO_2/C-2 shows a higher initial capacity of nearly 1481.71 mAh g^{-1} than the Co/C (1182.92 mAh g^{-1}). The galvanostatic charge/discharge profiles (Figure **S**6) depict that the Co@M-TiO_2/C-2 possesses longer plateaus and lower overpotential (ΔE) at 0.2 C than other samples, indicating the fast redox kinetics of LiPSs and the decreased electrochemical polarization. Figure 4b shows the rate performance of the cells at different rates of 0.2 C, 0.5 C, 1 C, and 2 C, respectively. The Co@M-TiO_2/C-2 exhibits high capacities of 1394.16 mAh g^{-1}, 1172.61 mAh g^{-1}, 1050.63 mAh g^{-1}, 855.53 mAh g^{-1} at 0.2 C, 0.5 C,1 C, 2 C, respectively, which is superior to the other three samples. Moreover, by comparing the discharge/charge curves of cells using Co@M-TiO_2/C-2 modified separator (Figure 4c) and Co/C modified separator (Figure **S**7) at different current densities, the Co@M-TiO_2/C-2 modified separator has a more stable platform and higher plateau capacity ratio than that of Co/C separator, indicating that the heterostructure formed by Co and TiO_2 facilitate the fast electrochemical reaction kinetics. The high S loading is a rigidity requirement for practical application, and the cycling stability of the batteries with Co@M-TiO_2/C-2 separator with a high loading of 4.4 mg cm^{-2} was tested (Figure 4d). The cell with Co@M-TiO_2/C-2 modified separator displays a high specific capacity of 775.17 mAh g^{-1} at 0.2 C, and after 100 cycles, the average attenuation rate per cycle is only 0.33 %, demonstrating excellent cycling stability under high S loading. Figure 4e shows the long-term cycling life at a high current density of 1 C. The cell with Co@M-TiO_2/C-2 modified separator exhibits a higher initial capacity of 1062.13 mAh g^{-1} after 300 cycles, with an average capacity attenuation rate of 0.118 %. The galvanostatic charge/discharge curves of Figure **S**8 show the Co@M-TiO_2/C-2 also has longer plateaus and lower overpotential at 1 C than other samples.

To reveal the above unique role of Co@M-TiO_2/C on electrochemical performance, a series of experiments were designed to evaluate the catalytic property, lithium-ion diffusion, and polarization. In the CV curves of symmetric batteries (Figure 5a), the cells with Co@M-TiO_2/C separators possess higher redox current response than the cells with Co/C separators, indicating the positive role of Co@M-TiO_2 heterostructure in catalyzing the redox conversion of LiPSs. The cell with Co@M-TiO_2/C-2 separator shows the highest redox current response, which is consistent with its best performance. In the cyclic voltammetry (CV) curves (Figure 5b), the potential difference between the reduction peak and the oxidation peak of Co@M-TiO_2/C-2 separator is lower than that of the Co/C, Co@M-TiO_2/C-1, and Co@M-TiO_2/C-3 separator. The battery with Co@M-TiO_2/C-2 separator also shows higher current density than that of the batteries using other separators. This indicates that the degree of polarization of Co@M-TiO_2/C-2 is smaller

Research Article
doi.org/10.1002/batt.202300516
Chemistry Europe
European Chemical Societies Publishing

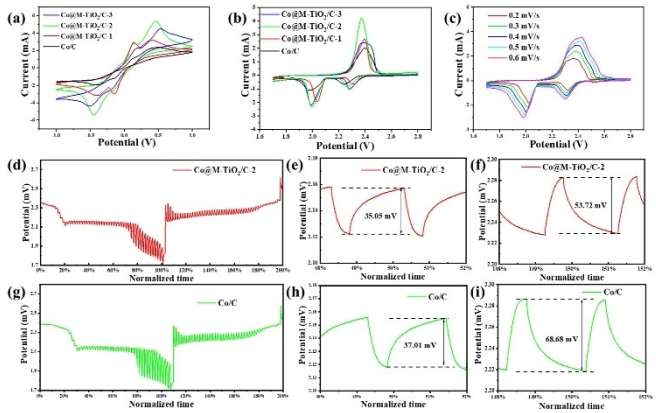

Figure 5. (a) CV curves of symmetric batteries with Co@M-TiO_2/C and Co/C separators. (b) CV curves of Li–S batteries with Co@M-TiO_2/C and Co/C modified separators at 0.1 mV s^{-1}. (c) CV curves of the cell with Co@M-TiO_2/C-2 separators under different scanning rates. The GITT image of Co@M-TiO_2/C-2 (d–f) and Co/C (g–i).

than that of other samples. Figure S9 shows the electrochemical impedance spectroscopy (EIS) of batteries with Co@M-TiO_2/C and Co/C separators, and the curves consist of a semicircle and a slope line, which correspond to the charge transfer resistance (R_{ct}) and the Warburg impedance, respectively. Compared with the Co/C separator, the R_{ct} of Co@M-TiO_2/C separators is a bit higher, which can be ascribed to the oxidization of MXene to TiO_2. In Figure 5c and Figure S10, the oxidation peaks of the cells with different separators move towards higher voltages with the increase of sweep rates, and the reductive peaks shift negatively. The slopes of different redox peaks of Co@M-TiO_2/C-2 are higher than those of Co/C, indicating that Co@M-TiO_2/C-2 has better diffusion kinetics. In the GITT curves of Co@M-TiO_2/C-2 and Co/C (Figure 5d–i), at the same depth of discharge, the relaxation voltage of Co@M-TiO_2/C-2 (35.05 mV) is smaller than that of Co/C (37.01 mV), while at the same depth of charge, the relaxation voltage of Co@M-TiO_2/C-2 (53.72 mV) is also smaller than that of Co/C (68.68 mV). This fully demonstrates that the polarization of Co@M-TiO_2/C-2 is smaller. Consequently, benefiting from the catalytic ability, rapid ion diffusion, and smaller polarization, the cells with Co@M-TiO_2/C-2 exhibit outstanding rate performance and cycling performance at high S loading, demonstrating its tremendous potential for Li–S battery applications.

Conclusions

In summary, a novel Co@M-TiO2/C heterostructure was successfully synthesized as a functional separator coating to trap polysulfide and accelerate redox kinetics for high-performance Li–S batteries. This structure has a large specific surface area and an interconnected porous carbon sheet structure, ensuring complete exposure of the active sites. The synergistic effect of Co and TiO_2 heterostructures on the adsorption and catalysis of LiPSs is stronger compared to Co alone, effectively inhibiting the shuttle effect and accelerating redox kinetics. As a result, the initial capacity, rate capability, and cycling performance under high loading are all enhanced. This work lays the groundwork for studying the heterogeneous structure formed by MXene-derived polyphase TiO_2 and metal elements in Li–S batteries.

Materials and Methods

Preparation of Co@M-TiO_2/C composites

Typically, 342 mg of cobalt (II) chloride hexahydrate ($CoCl_2 \cdot 6H_2O$), 880 mg of folic acid, and different amounts of $Ti_3C_2T_x$ MXenes (15 mg, 30 mg, and 45 mg) were dissolved into 50 ml of a mixture of ethanol and deionized water (volume ratio of 3:2). Then, the mixed solution was moved to a Teflon-lined autoclave and the hydrothermal reaction was carried out at 140 °C for 2 hours. The samples were washed three times, completely frozen, and vacuum freeze-dried for 12 hours. The puffy brown-green powder was transferred in a tube furnace, heated to 800 °C at a heating rate of 5 °C/min under an argon atmosphere, and kept warm for 2 hours to obtain the target product, which was marked as Co@M-TiO_2/C-x (x:1, 2, and 3, representing the different amounts of $Ti_3C_2T_x$ MXenes respectively.). Then the control sample Co/C was also prepared by the same method but without adding MXenes.

The fabrication of Co@M-TiO_2/C and Co/C modified separator

The Co@M-TiO_2/C and polyvinylidene difluoride (PVDF) were well mixed into a homogenous slurry (9:1) in N-methyl-2-pyrrolidone (NMP) solvent and then coated onto the PP separator, vacuum dried at 65 °C overnight. The average surface load of the prepared modified separator is about 0.314 mg cm^{-2}.

Preparation of sulfur composites

Ketjen black (KB) and sublimated sulfur powder were mixed evenly with a mass ratio of 1:3, and KB/S powder was obtained by heat treatment at 155 °C for 12 h.

Material characterization

The phase information of Co@M-TiO_2/C and Co/C in the angle range of 5°~80° was explored by XRD (Cu Ka radiation, k = 1.5405 A). The microstructure and lattice structure of Co@M-TiO_2/C and Co/C were analyzed by scanning electron microscope (SEM, Nova Nano SEM450, 15 K eV), transmission electron microscope (TEM, JEOL JEM 2100F) and additional energy dispersive X-ray spectrometer (EDX, Oxford Instruments, and EDAX). The elemental forms of Co@M-TiO_2/C and Co/C were dug into by X-ray photoelectron spectroscopy (XPS, ESCALAB250).

Electrochemical measures

KB/S powder, KB, and PVDF were mixed evenly according to the mass ratio of 8:1:1, dissolved in N-methyl pyrrolidone (NMP) to form a slurry and then were coated on aluminum foil, dried in a vacuum oven at 60 °C overnight to obtain the S cathode. The coin cells (CR-2032) were assembled with the sulfur cathode, modified separator, electrolyte (1 M lithium bis (trifluoromethane sulfonimide) and 0.1 M Lithium nitrate ($LiNO_3$) in a mixed solvent of 1,2-dimethoxyethane and 1,3-dioxolane (volume ratio of 1: 1)), and lithium anode in a glove box under an argon atmosphere. ($H_2O \leq$

0.01 ppm, $O_2 \leq 0.01$ ppm). The amount of electrolyte used in each cell was 15 μL. The electrochemical workstation (CHI 760E) was used to obtain the cyclic voltammetry curves (CV) at a scan rate of 0.2~0.6 mV s^{-1} and a working voltage from 1.7 to 2.8 V. The NEWARE battery measurement system was applied to test the electrochemical properties of Co@M-TiO_2/C and Co/C modified batteries.

Acknowledgements

J. S. would like to acknowledge the financial support of the Natural Science Foundation of Shandong Province, China (No. ZR2021QE192). X. Z. thanks the National Natural Science Foundation of China (22105059), the Natural Science Foundation of Hebei Province (B2023204006), and the Youth Top-notch Talent Foundation of Hebei Provincial Universities (BJK2022023). Open Access publishing facilitated by University of Technology Sydney, as part of the Wiley - University of Technology Sydney agreement via the Council of Australian University Librarians.

Conflict of Interests

The authors declare no conflict of interest.

Data Availability Statement

The data that support the findings of this study are available from the corresponding author upon reasonable request.

Keywords: Li–S batteries · heterostructure · shuttle effect · redox kinetics · separator

[1] S. Zhou, J. Shi, S. Liu, G. Li, F. Pei, Y. Chen, J. Deng, Q. Zheng, J. Li, C. Zhao, I. Hwang, C.-J. Sun, Y. Liu, Y. Deng, L. Huang, Y. Qiao, G.-L. Xu, J.-F. Chen, K. Amine, S.-G. Sun, H.-G. Liao, *Nature* **2023**, *621*, 75–81.
[2] J.-C. Liu, L.-L. Ma, S. Li, L.-L. Hou, X.-R. Qi, Y.-Q. Wen, G.-P. Hu, N. Wang, Y. Zhao, X.-X. Zhao, *Rare Met.* **2023**, *42*, 3378.
[3] Y.-N. Zhang, C.-Y. Su, J.-L. Chen, W.-H. Huang, R. Lou, *Rare Met.* **2022**, *42*, 769–796.
[4] Y. Zhang, L. Zhang, P. Guo, C. Zhang, X. Ren, Z. Jiang, J. Song, C. Shi, *Nano Res.* **2023**,doi: 10.1007/s12274-023-6065-4.
[5] W.-D. Liu, X. Tang, J.-A. Feng, C.-Y. Zhang, H. Liu, C. Shi, X.-X. Zhao, J.-J. Song, *Rare Met.* **2023**, DOI: 10.1007/s12598-023-02417-7.
[6] C. Liu, C. Mo, L. Zhong, X. Gong, Y. Zhang, X. Wang, F. Yang, J. Li, J. Lu, D. Yu, *Angew. Chem. Int. Ed.* **2023**, *62*, 202312016–202312025.
[7] Y. X. Yin, S. Xin, Y. G. Guo, L. J. Wan, *Angew. Chem. Int. Ed.* **2013**, *52*, 13186–13200.
[8] A. Manthiram, Y. Fu, S.-H. Chung, C. Zu, Y.-S. Su, *Chem. Rev.* **2014**, *114*, 11751–11787.
[9] K. Liu, H. Zhao, D. Ye, J. Zhang, *Chem. Eng. J.* **2021**, *417*, 129309–129323.
[10] Y. Liu, Y. Elias, J. Meng, D. Aurbach, R. Zou, D. Xia, Q. Pang, *Joule* **2021**, *5*, 2323–2364.
[11] T. Yang, J. Xia, Z. Piao, L. Yang, S. Zhang, Y. Xing, G. Zhou, *ACS Nano* **2021**, *15*, 13901–13923.
[12] L. Ma, X. Zhou, J. Sun, P. Zhang, B. Hou, S. Zhang, N. Shang, J. Song, H. Ye, H. Shao, Y. Tang, X. Zhao, *J. Energy Chem.* **2023**, *82*, 268.
[13] C. Dai, L. Hu, X. Li, Q. Xu, R. Wang, H. Liu, H. Chen, S.-J. Bao, Y. Chen, G. Henkelman, C. M. Li, M. Xu, *Nano Energy* **2018**, *53*, 354–361.
[14] C. Zhao, G. L. Xu, T. Zhao, K. Amine, *Angew. Chem. Int. Ed.* **1020**, *59*, 17634–17640.
[15] H. Ye, Y. Li, *Nano Res. Energy* **2022**, *1*, e9120012.
[16] Q. Wu, X. Zhao, T. Zhou, A. Jia, Y. Luo, J. Li, F. Wu, *J. Energy Storage* **2023**, *72*, 108596–108604.
[17] D. Zhu, T. Long, B. Xu, Y. Zhao, H. Hong, R. Liu, F. Meng, J. Liu, *J. Energy Chem.* **2021**, *57*, 41–60.
[18] X. Qi, L. Huang, Y. Luo, Q. Chen, Y. Chen, *J. Colloid Interface Sci.* **2022**, *628*, 896–910.
[19] Z. Lin, J. Feng, W. Liu, L. Yin, W. Chen, C. Shi, J. Song, *Batteries* **2023**, *9*, 296–307.
[20] K. Xu, X. Liang, L.-L. Wang, Y. Wang, J.-F. Yun, Y. Sun, H.-F. Xiang, *Rare Met.* **2021**, *40*, 2810–2818.
[21] J. Liu, M. Liu, C. Wang, Q. Li, J. Li, Y. Chen, Z. Hong, F. Song, L. Bai, F. Zeng, *Int. J. Energy Res.* **2021**, *45*, 16551–16564.
[22] Y. Liu, H. Wei, X. Zhai, F. Wang, X. Ren, Y. Xiong, O. Akiyoshi, K. Pan, F. Ren, S. Wei, *Mater. Des.* **2021**, *211*, 110171–110204.
[23] H. Ding, Q. Zhang, Z. Liu, J. Wang, R. Ma, L. Fan, T. Wang, J. Zhao, J. Ge, X. Lu, X. Yu, B. Lu, *Electrochim. Acta* **2018**, *284*, 314–320.
[24] Z. Li, C. Zhou, J. Hua, X. Hong, C. Sun, H. W. Li, X. Xu, L. Mai, *Adv. Mater.* **2020**, *32*, 1907444–1907451.
[25] X. Liu, J. Q. Huang, Q. Zhang, L. Mai, *Adv. Mater.* **2017**, *29*, 1601759–1601783.
[26] R. Xu, H. Tang, Y. Zhou, F. Wang, H. Wang, M. Shao, C. Li, Z. Wei, *Chem. Sci.* **2022**, *13*, 6224–6232.
[27] B. Yan, X. Li, W. Xiao, J. Hu, L. Zhang, X. Yang, *J. Mater. Chem. A* **2020**, *8*, 17848–17882.
[28] J.-L. Yang, D.-Q. Cai, Q. Lin, X.-Y. Wang, Z.-Q. Fang, L. Huang, Z.-J. Wang, X.-G. Hao, S.-X. Zhao, J. Li, G.-Z. Cao, W. Lv, *Nano Energy* **2022**, *91*, 106669–106677.
[29] M. Luo, Y. Bai, R. Sun, M. Qu, M. Wang, Z. Yang, Z. Wang, W. Sun, K. Sun, *J. Energy Chem.* **2022**, *73*, 407–415.
[30] S. Yu, W. Cai, L. Chen, L. Song, Y. Song, *J. Energy Chem.* **2021**, *55*, 533–548.
[31] J. Feng, C. Shi, H. Dong, C. Zhang, W. Liu, Y. Liu, T. Wang, X. Zhao, S. Chen, J. Song, *J. Energy Chem.* **2023**, *86*, 135–145.
[32] S. K. Kumar, M. M. Gaikwad, P. Rani, A. D. Pathak, C. S. Sharma, *Electrochim. Acta* **2022**, *401*, 139466–139477.
[33] G. Liu, C. Yuan, P. Zeng, C. Cheng, T. Yan, K. Dai, J. Mao, L. Zhang, *J. Energy Chem.* **2022**, *67*, 73–81.
[34] S. Liu, J. Li, X. Yan, Q. Su, Y. Lu, J. Qiu, Z. Wang, X. Lin, J. Huang, R. Liu, B. Zheng, L. Chen, R. Fu, D. Wu, *Adv. Mater.* **2018**, *30*, 1706895–1706903.
[35] C. Zhang, J. Feng, X. Guo, J. Zhang, W. Zhang, L. Zhang, J. Song, G. Shao, G. Wang, *Appl. Phys. Lett.* **2023**, *122*, 193901–193906.
[36] Z.-L. Tan, J.-X. Wei, Y. Liu, F. u. Zaman, W. Rehman, L.-R. Hou, C.-Z. Yuan, *Rare Met.* **2021**, *41*, 775–797.
[37] L. Jiao, C. Zhang, C. Geng, S. Wu, H. Li, W. Lv, Y. Tao, Z. Chen, G. Zhou, J. Li, G. Ling, Y. Wan, Q. H. Yang, *Adv. Energy Mater.* **2019**, *9*, 1900219–1900227.

Manuscript received: November 5, 2023
Revised manuscript received: December 15, 2023
Accepted manuscript online: December 20, 2023
Version of record online: January 9, 2024